

## Time-resolved synchrotron X-ray diffraction study of the dehydration behavior of chalcophanite

JEFFREY E. POST<sup>1,\*</sup> AND PETER J. HEANEY<sup>2</sup>

<sup>1</sup>Department of Mineral Sciences, Smithsonian Institution, PO Box 37012, Washington, D.C. 20013-7012, U.S.A.

<sup>2</sup>Department of Geosciences, Penn State University, University Park, Pennsylvania 16802, U.S.A.

### ABSTRACT

Time-resolved synchrotron X-ray powder diffraction data were used to investigate the dehydration behavior of the chalcophanite ( $\text{ZnMn}_3\text{O}_7 \cdot 3\text{H}_2\text{O}$ ) structure from 300 to 1060 K. Rietveld refinements revealed two obvious phase changes, at  $\sim 450$  and  $\sim 950$  K, corresponding to the dehydration of chalcophanite followed by transformation to a spinel structure (Mn-hetaerolite). Only small changes were observed in the chalcophanite unit cell from RT to  $\sim 438$  K; the volume increased by  $\sim 0.8\%$ , mostly caused by thermal expansion of  $\sim 0.5\%$  along  $c$ . Above  $\sim 427$  K, the interlayer water molecules were lost, resulting in a collapse of the interlayer spacing from  $\sim 7$  to  $\sim 4.8$  Å. The newly formed anhydrous phase ( $\text{ZnMn}_3\text{O}_7$ ) retained chalcophanite's  $R\bar{3}$  space group and  $a$  dimension, but the  $c$  dimension decreased from  $\sim 21$  to  $14.3$  Å, and the Zn coordination changed from octahedral to tetrahedral. Above  $\sim 775$  K the anhydrous chalcophanite began to transform to a spinel structure, corresponding to a Mn-rich hetaerolite [ $(\text{Zn}_{0.75}\text{Mn}_{0.25}^{2+})\text{Mn}_2^{3+}\text{O}_4$ ]. By  $\sim 973$  K the transformation was complete. The diffraction patterns did not show a significant increase in background during the transformation, indicating that the reaction did not involve transient amorphization. The phase change was likely triggered by loss of 1.25 of seven O atoms in the original anhydrous chalcophanite structure with a corresponding reduction of  $\text{Mn}^{4+}$  to  $\text{Mn}^{3+}$  and  $\text{Mn}^{2+}$ .

**Keywords:** Chalcophanite, hetaerolite, birnessite, Rietveld, synchrotron

### INTRODUCTION

Chalcophanite is a hydrated zinc-manganese oxide that is one of a family of predominantly tetravalent Mn oxide minerals with layer structures (phyllomanganates) that also includes birnessite, ranciéite, takanelite, and lithiophorite. It is constructed of sheets of  $\text{Mn}^{4+}$ -O octahedra with the Zn cations and water molecules located between the layers. It is found in oxidized Mn deposits that also contain Zn, as exemplified by its type locality (Sterling Hill in the Franklin Mining District, New Jersey). Recently, Mg- and Ni-rich structural analogs to chalcophanite have been reported, which are jianshuiite (Guiyin et al. 1992) and ernienickelike (Grice et al. 1994), respectively.

Recent interest in the behavior of chalcophanite is motivated by its structural similarity to members of the birnessite family. Birnessite-like layer minerals are common Mn oxides in soils, stream deposits, and ocean-floor ferromanganese crusts and nodules (Taylor et al. 1964; McKenzie 1976; Burns and Burns 1977; Potter and Rossman 1979; Post 1999). Birnessite-like layer structures are also used as cathodic materials in rechargeable Li batteries and are being developed as ion-exchange compounds and catalysts for industrial use (Golden et al. 1986; Bach et al. 1995; Cai et al. 2002). Because cations are readily adsorbed on or incorporated into the birnessite structure (McKenzie 1976), birnessites play an important role in the sequestration and release of nutrients and toxic elements in surficial environments. For

example, Toner et al. (2006) have demonstrated that the biogeochemical cycling of Zn is controlled by sorption onto birnessite minerals in soils and streams.

Despite their importance as battery and exchange materials and their active role in geological systems, birnessite-like phases are challenging to investigate because they tend to occur as fine-grained, poorly crystalline masses. Chalcophanite is unusual in the birnessite family in that it typically is well crystallized, commonly forming crystals up to several millimeters in diameter. Consequently it serves as an excellent proxy for better understanding the structures and behaviors of the broader group of birnessite-like phases.

The chalcophanite structure was originally described by Wadsley (1955) using a triclinic unit cell, but a later study by Post and Appleman (1988) revealed that, in fact, the correct symmetry is  $R\bar{3}$ . The structure consists of sheets of edge-sharing  $\text{Mn}^{4+}$ -O<sub>6</sub> octahedra alternating with layers of Zn cations and water molecules in the stacking sequence:  $\cdots\text{Mn-O-Zn-H}_2\text{O-Zn-Mn}\cdots$  (Fig. 1). One out of every seven octahedral sites in the Mn-O sheet is vacant, and the Zn cations are located above and below the vacancies. The vacant Mn sites are fully ordered. The  $\sim 7$  Å spacing between the Mn-O sheets is one of the defining characteristics of birnessite-like phases. (There is an analogous group of birnessite-like phases within the “buserite” family with  $\sim 10$  Å layer spacings due to an additional water layer.) Synthetic birnessite analogs crystallize in both triclinic and hexagonal forms, depending upon pH and composition. In the triclinic phases, typically  $\text{Mn}^{3+}$  cations, rather than vacancies, offset the

\* E-mail: postj@si.edu

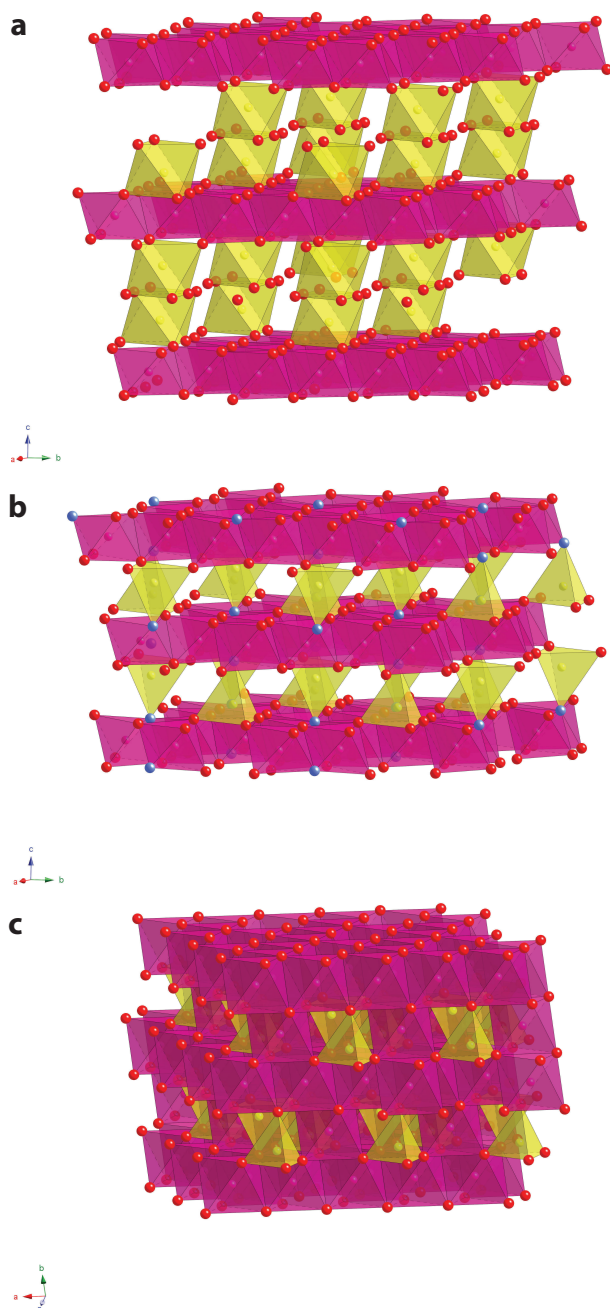


**FIGURE 1.** Structure drawings of: (a) chalcophanite, (b) anhydrous chalcophanite, and (c) Mn-rich hetaerolite. Mn-O octahedra are colored pink, and Zn-O polyhedra are yellow. The O atoms are indicated by red and blue [O(3)] spheres. For all three structures the *c* axis is vertical. (Color online.)

charges of the interlayer cations (Post et al. 2002; Lanson et al. 2002). Synthetic hexagonal birnessites, on the other hand, do not contain  $\text{Mn}^{3+}$ , but in contrast with chalcophanite, the  $\text{Mn}^{4+}$  vacancies are disordered in the Mn-O octahedral sheets (Drits et al. 1997; Post et al. 2008). The mineral birnessite,  $(\text{Na,Ca,Mn}^{2+})\text{Mn}_7\text{O}_{14} \cdot 2.8\text{H}_2\text{O}$ , was first described by Jones and Milne (1956). Natural samples were also found to contain trace amounts of a

variety of cations, including Co, Ni, and Pb (McKenzie 1977). Various synthetic birnessite-like structures containing almost every alkali and alkaline earth element, as well as many of the transition metals, have been produced in the laboratory, and most readily undergo cation exchange (e.g., McKenzie 1971; Golden et al. 1986; Lopano et al. 2007). Interestingly, analyses of chalcophanite samples from various localities show only minor amounts of cations other than Zn. This suggests that the Zn cation is particularly well suited for growing a well-crystallized birnessite-like phase at the proper environmental conditions.

Ranciéite is a Ca-rich birnessite that is commonly associated with biologically precipitated Mn oxides, and it also occurs in oxidized zones of Mn deposits and in low-temperature hydrothermal veins. Recent studies (Post et al. 2008) have shown that it has a hexagonal structure similar to that of chalcophanite, but apparently with disordered vacancies in the Mn-O octahedral sheets.

All birnessite-like phases contain water molecules in addition to cations in the interlayer regions. In situ infrared spectroscopy studies of the dehydration behaviors of various cation-exchanged birnessite phases by Johnson and Post (2006) suggest that cation hydration energies, and consequently, cation-water interactions are important factors in the relative stabilities and in the exchange behaviors of birnessite phases. Experimentally based descriptions of the interlayer region, however, and particularly of the roles played by the water molecules, are severely limited by the poor crystallinity of most birnessite-like materials. Density functional theory calculations by Kwon et al. (2009) indicate that the hydration state of Zn in a chalcophanite-like phase significantly affects the structural stability. As water loss occurs when birnessite phases are heated even to relatively low temperatures ( $<200^\circ\text{C}$ ), structural changes related to dehydration will directly impact the material behavior in near-surface environments.

In the current study we used time-resolved synchrotron X-ray powder diffraction and Rietveld refinements to better explore the interactions among the water molecules, interlayer cations, and the MnO octahedral sheets in chalcophanite. Here we present the results of a series of refinements of the chalcophanite structure over the temperature range 300 to  $\sim 1060$  K. These dehydration data provide, for the first time, a direct look at changes in the structure with increasing temperature as it undergoes multiple phase changes, including formation of a stable intermediate dehydrated layer structure.

## EXPERIMENTAL DETAILS

The chalcophanite sample used for this study, NMNH C1814 from Sterling Hill, New Jersey, is the same as that used for the single-crystal X-ray diffraction study by Post and Appleman (1988). They reported that the composition was very close to  $\text{ZnMn}_7\text{O}_{14} \cdot 3\text{H}_2\text{O}$ . The sample used for X-ray diffraction was hand-ground under acetone in an agate mortar and passed through a 325-mesh sieve and loaded into a 0.5 mm quartz-glass capillary for the synchrotron XRD study. XRD data were collected at beamline X7B of the National Synchrotron Light Source (NSLS), Brookhaven National Laboratory (BNL), using a wavelength of 0.9273 Å and a MAR345 full image plate detector.

The heating experiment was performed in air using a Blake Instruments furnace with a Pt-13%Rh coiled wire yoke encased in  $\text{ZrO}_2$  cement (Brown et al. 1973). The temperature was varied with an Omega controller and monitored with a Chromel-Alumel thermocouple located  $\sim 2$  mm from the specimen. The actual sample temperature was determined for the range 298 to 1273 K by a variety of phase and melting transitions and by the placement of an additional thermocouple in the sample position. The highly linear relationship between the observed and actual temperatures ( $R^2 = 0.983$ ) allowed us to calculate a calibration curve with an

estimated error of  $\pm 5$  K for a given temperature. Temperature-resolved data from 300 to 1063 K were collected as a series of 120 s exposures. The temperature was increased continuously at 8.5 K/min and measurements were obtained every  $\sim 28$  K, owing to down time for repositioning of the sample and reading the imaging plate; thus, each exposure encompassed a temperature range of  $\sim 17$  K. During each exposure the sample was rotated through a  $120^\circ$  angle. Preferred orientation of the powder was eliminated through a combination of the specimen rotation, use of a capillary sample holder, and full intensity integration of the diffraction rings, as obtained using the program Fit2D (Hammersley et al. 1996) with a polarization factor of 0.93.

Rietveld refinements were performed using the general structure analysis system (GSAS) of Larson and Von Dreele (2006) and EXPGUI interface by Toby (2001). The RT starting chalcophanite structural parameters were taken from Post and Appleman (1988). The model for the "anhydrous" chalcophanite was derived with assistance from the program "Crystal Cracker" (Build 189, K. Leinenweber, unpublished), which allowed us to determine starting unit-cell parameters. Difference-Fourier maps were calculated using the MnO octahedral layers to locate the Zn atoms in the interlayer region. The diffraction pattern backgrounds were fit using a linear interpolation function. Peak profiles were modeled by a pseudo-Voigt profile function as parameterized by Thompson et al. (1987) and microstrain anisotropic broadening terms by Stephens (1999). Displacement factors for chalcophanite were fixed to values reported by Post and Appleman (1988), and subsequently refined for the anhydrous phases.

During the initial cycles of refinement, only the background, scale, peak profile, and unit-cell parameters were allowed to vary. After convergence, all atom positions, displacement factors (for anhydrous phases), and appropriate occupancy factors, e.g., of the O atoms of the H<sub>2</sub>O molecules and Zn site in the anhydrous phases, were refined.

The final refinement parameters for 300 K chalcophanite, the intermediate anhydrous phase (540 K), and Mn-hetaerolite (994 K) are listed in Table 1. The refined chalcophanite atom positions did not differ significantly from those reported by Post and Appleman (1988) and therefore are not listed here. Atom positions for the anhydrous chalcophanite were similar at all temperatures; therefore, only the values determined at 540 K are reported in Table 2, along with those for Mn-hetaerolite at 994 K. Selected bond distances for anhydrous chalcophanite and Mn-hetaerolite are reported in Table 3. The final observed, calculated, and difference patterns for chalcophanite (300 K), anhydrous chalcophanite (540 K), and Mn-hetaerolite (994 K) are plotted in Figure 2. The standard deviations calculated by GSAS for the lattice parameters are likely lower than the true errors (Post and Bish 1989). (A CIF is available<sup>1</sup>.)

## RESULTS AND DISCUSSION

The synchrotron powder X-ray diffraction patterns collected over the range 300 to 1060 K are plotted in Figure 3. The plot reveals two obvious phase changes, at  $\sim 450$  and  $\sim 950$  K, corresponding to the dehydration of chalcophanite followed by transformation to a spinel structure, Mn-hetaerolite, as discussed below.

### Chalcophanite (ZnMn<sub>3</sub>O<sub>7</sub>·3H<sub>2</sub>O) dehydration

The Rietveld refined structure for chalcophanite at room temperature is not significantly different than that reported from the single-crystal diffraction study of Post and Appleman (1988). The Mn-O distances correspond to within 0.02 Å, giving an indication of the general accuracy of the Rietveld structures determined in this study. Some noteworthy aspects of the structure that were also discussed by Post and Appleman (1988) are (1) the Mn-O octahedra are distorted, with bond distances ranging from 1.86 to 1.97 Å, caused by displacement of the Mn toward the vacancy in the octahedral sheet; (2) the mean Mn-O distance is 1.91 Å, indicating that all Mn is Mn<sup>4+</sup>; and (3) the Zn cations occupy

**TABLE 1.** Final Rietveld refinement parameters for chalcophanite, anhydrous chalcophanite, and Mn-hetaerolite

	Chalcophanite (300 K)	Anhydrous chalcophanite (540 K)	Mn-hetaerolite (994 K)
Space group	$R\bar{3}$	$R\bar{3}$	$I4_1/amd$
Unit cell			
<i>a</i> (Å)	7.5437(1)	7.5482(4)	5.75337(26)
<i>b</i> (Å)	7.5437(1)	7.5482(4)	5.75337(26)
<i>c</i> (Å)	20.8182(7)	14.2955(13)	9.3162(6)
<i>V</i> (Å <sup>3</sup> )	1026.0(1)	705.37(1)	308.38(4)
Refinement			
No. of data points	1687	1687	2050
No. of reflections	210	124	45
Diffraction range (2 $\theta$ )	13.5–47.3	13.5–47.3	8–49
No. of variables	42	46	37
<i>R</i> (F <sup>2</sup> )	0.042	0.056	0.025
<i>R</i> <sub>wp</sub>	0.014	0.017	0.013
$\chi^2$	0.94	1.12	1.94

**TABLE 2.** Atomic coordinates and isotropic displacement factors for anhydrous chalcophanite and Mn-hetaerolite

Atom	<i>x</i>	<i>y</i>	<i>z</i>	Site occupancy factor	<i>U</i> <sub>iso</sub>
<b>Anhydrous chalcophanite (540 K)</b>					
Mn	0.7193(6)	0.5799(6)	0.00079(31)	1.0	0.0142(7)
Zn	0	0	0.1308(5)	1.0	0.0142(7)
O(1)	0.5233(23)	0.6291(29)	0.0678(10)	1.0	0.0318(18)
O(2)	0.2648(24)	0.2104(24)	0.0779(1)	1.0	0.0318(18)
O(3)	0	0	0.7292(15)	1.0	0.0318(18)
<b>Mn-hetaerolite (994 K)</b>					
Mn	0	0.5	0.5	1.0	0.0152(7)
Zn	0	0.25	0.875	0.941(2) <sup>a</sup>	0.0179(6)
O	0	0.4749(4)	0.2552(2)	1.0	0.0300(9)

Note: *U*<sub>iso</sub> for O atoms in anhydrous chalcophanite were constrained to be the same; coordinates are for origin choice at 2/*m* [add (0, 1/4, -1/6) to shift to origin at -4*m*2].

<sup>a</sup> Site also contains Mn but was refined as Zn.

**TABLE 3.** Selected bond lengths for anhydrous chalcophanite and Mn-hetaerolite structures (Å)

	Anhydrous chalcophanite (540 K)	Mn-hetaerolite (994 K)
Mn-O(1)	1.858(17)	1.93515(9) × 4
Mn-O(1)	1.948(14)	2.28510(14) × 2
Mn-O(1)	1.978(17)	
Mn-O(2)	1.872(14)	
Mn-O(2)	1.897(14)	
Mn-O(3)	1.914(10)	
<Mn-O>	1.91	2.05
Zn-O(2)	1.978(15) × 3	1.99434(7) × 4 <sup>a</sup>
Zn-O(3)	2.001(18)	
<Zn-O>	1.99	1.994

<sup>a</sup> Site contains  $\sim 0.75$  Zn and 0.25 Mn.

sites above and below the vacancies in the octahedral sheets and are coordinated to three O atoms and three water oxygen atoms.

The results of the heating study show only small changes in the chalcophanite unit cell from RT to  $\sim 438$  K (Fig. 4). The volume increased by  $\sim 0.8\%$ , mostly caused by thermal expansion of  $\sim 0.5\%$  along *c*; the value of *a* increased only  $\sim 0.1\%$ . Between  $\sim 438$  and 473 K, the volume increased more rapidly by an additional 0.8%, primarily caused by a  $\sim 1.0\%$  increase along *c*. This latter change in volume corresponds to the period of maximum water evolution, as discussed below. Our structure refinements revealed a gradual decrease in the occupancy factor for the water oxygen atom, starting above  $\sim 416$  K, giving values of 0.85 at 416 K, 0.75 at 427 K, 0.69 at 438 K, and 0 above  $\sim 450$  K. The changes in occupancy factor correlated with drops in the intensity of the 001 diffraction peak in Figure 3, with the first apparent change at 416 K. The 001 peak disappeared by  $\sim 473$  K. This

<sup>1</sup> Deposit item AM-14-1012, CIF. Deposit items are stored on the MSA web site and available via the *American Mineralogist* Table of Contents. Find the article in the table of contents at GSW (ammin.geoscienceworld.org) or MSA (www.minsocam.org), and then click on the deposit link.

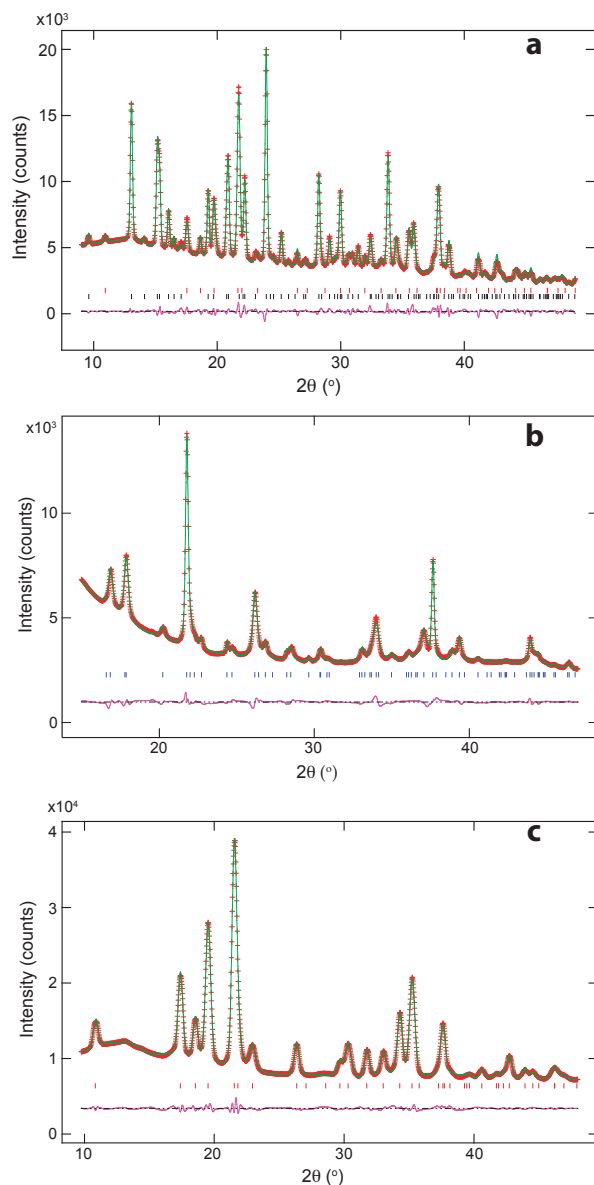


**FIGURE 2.** Final observed (red crosses), calculated (green solid line), and difference (purple below) powder X-ray diffraction patterns from the Rietveld refinement for: (a) chalcophanite, (b) anhydrous chalcophanite, and (c) Mn-rich hetaerolite. The Bragg reflections are marked by the set of small vertical lines. (Color online.)

transition is consistent with the first appearance of anhydrous chalcophanite at 427 K from the Rietveld refinements, and we infer that chalcophanite had completely transformed by 473 K. The structure refinements did not show any significant changes in chalcophanite Mn-O distances or occupancy factors other than for the water oxygen atom during dehydration.

#### Anhydrous chalcophanite ( $\text{ZnMn}_3\text{O}_7$ )

As chalcophanite was heated above  $\sim 427$  K, the interlayer water molecules were lost, resulting in a collapse of the interlayer spacing from  $\sim 7$  to  $\sim 4.8$  Å. The newly formed anhydrous

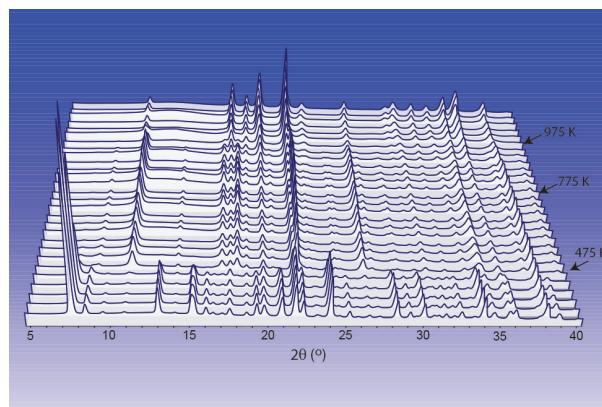


**FIGURE 3.** Synchrotron powder X-ray diffraction patterns vs. temperature from RT (front) to 1060 K. (Color online.)

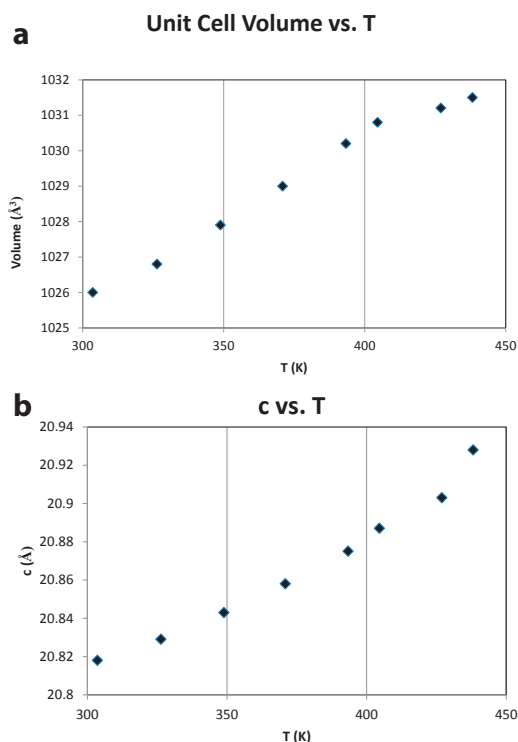


**FIGURE 4.** Plots of: (a) unit-cell volume and (b)  $c$  for chalcophanite for the temperature range 300 to 438 K. Calculated e.s.d. values fall within the areas of the plotting symbols. (Color online.)

phase retains chalcophanite's  $R\bar{3}$  space group and  $a$  dimension, but has a  $c$  dimension of 14.3 Å instead of  $\sim 21$  Å. The fraction of anhydrous chalcophanite increased as the sample was heated above 427 K until at  $\sim 473$  K no chalcophanite remained. The anhydrous chalcophanite remained the stable phase until  $\sim 775$  K, above which, as is discussed below, it transformed to a Mn-rich hetaerolite that has the spinel structure.

The existence of anhydrous chalcophanite was first noted by Dasgupta (1974) based on results of heating chalcophanite single crystals. His diffraction and differential thermogravimetric

experiments indicated a transformation of chalcophanite to the anhydrous phase at  $\sim 473$  K, which agrees well with the results of the present study. Although he reported unit-cell parameters that are close to the values determined here, he was not able to determine a structure for the anhydrous phase.

The structure determined from our Rietveld study for anhydrous chalcophanite is shown in Figure 1. The obvious difference from the chalcophanite structure is the loss of the water molecules from the interlayer region and consequent collapse of the spacing between the octahedral sheets. The Mn-O distances calculated from the refined structure for the anhydrous phase are not significantly different from those in chalcophanite, ranging from 1.86 to 1.98 Å, with a mean value of 1.91 Å (Table 3), indicating that the Mn oxidation state is still tetravalent, and that the MnO octahedral sheets are essentially the same in both phases. The calculated bond valence sum for Mn (Brown and Altermatt 1985), using bond distances in Table 3, is 3.93. The Zn atoms remain in the interlayer region, positioned above and below the vacancies in the MnO octahedral sheets, but they are tetrahedrally coordinated to O atoms in the sheets, bonded to three O(2) above and one O(3) below. This coordination differs from the octahedral coordination of Zn in chalcophanite, to three O atoms in the octahedral sheet and three water oxygen atoms in the interlayer. The Zn-O distances range from 1.98 Å ( $\times 3$ ) to 2.00 Å, and they correspond well with the predicted tetrahedral bond distance of 1.98 Å, using the ionic radii of Shannon (1976). The bond valence sum for Zn is 1.87. The change in Zn coordination from octahedral to tetrahedral during dehydration is consistent with modeling calculations by Kwon et al. (2009) for a hypothetical monohydrate chalcophanite that shows Zn only in tetrahedral coordination. The particular flexibility of Zn cations to adopt octahedral or tetrahedral coordination might explain why chalcophanite forms a stable anhydrous phase, whereas birnessite-like materials having other interlayer cations, e.g., Na, Ba, Cs, Ca, etc. generally dehydrate to disordered/amorphous intermediate phases before transforming to spinel-like compounds (unpublished research).

#### Mn-rich hetaerolite [(Zn<sub>0.75</sub>Mn<sub>0.25</sub><sup>2+</sup>)Mn<sub>2</sub><sup>3+</sup>O<sub>4</sub>]

Above  $\sim 775$  K the anhydrous chalcophanite began to transform to a spinel structure, corresponding to a Mn-rich hetaerolite, and by  $\sim 973$  K the transformation was complete. The diffraction patterns did not show a significant increase in background during the transformation, indicating that the reaction did not involve transient amorphization. The phase change is associated with the reduction of Mn<sup>4+</sup> to Mn<sup>3+</sup> and Mn<sup>2+</sup>, with a corresponding loss of 1.25 of seven O atoms from the original anhydrous chalcophanite structure. The Rietveld refinements of the O atom occupancy factors for anhydrous chalcophanite as it was heated above  $\sim 700$  K showed a gradual decrease for the O(3) value from 0.94 to 0.76 at 845 K, while the values for O(1) and O(2) stayed close to 1.0, suggesting that most of the O loss during the transformation was O(3). We note that O(3) is structurally distinct from O(1) and O(2) in anhydrous chalcophanite. Each O(1) anion coordinates only to three Mn octahedral sites, and the O(2) anions serve as the basal O atoms of the Zn tetrahedra that are shared with the Mn octahedral sheet. Therefore, the O(2) anions each coordinate to 2 Mn cations and 1 Zn cation.

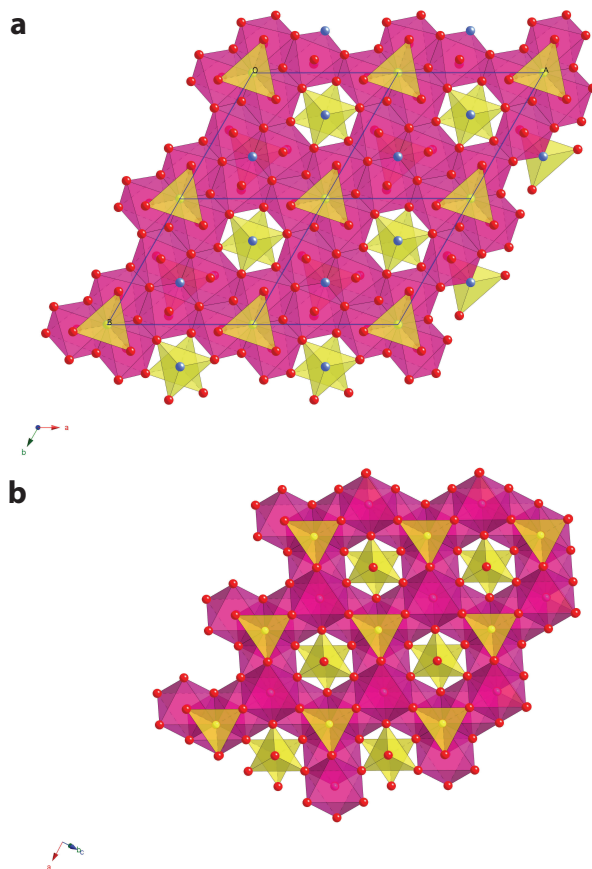


**FIGURE 5.** Polyhedral structure drawings for: (a) anhydrous chalcophanite and (b) Mn-rich hetaerolite projected down *c*. Mn-O octahedra are colored pink, and Zn-O polyhedra are yellow. The O atoms are indicated by red and blue [O(3)] spheres. (Color online.)

The O(3) anions are the apical O atoms of the Zn tetrahedra, and thus each O(3) anion is bonded to 3 Mn cations and 1 Zn cation. We presume that increasing thermal vibrations rupture Mn-O bonds, resulting in the selective loss of the O(3) anion as O<sub>2</sub> and the consequent reduction of Mn<sup>4+</sup> by electrons released as O<sup>2-</sup> is oxidized to O<sub>2</sub>. The Mn<sup>2+</sup> and Mn<sup>3+</sup> cations migrate to the interlayer as the structure transforms to Mn-rich hetaerolite. When the structures of hetaerolite and anhydrous chalcophanite are viewed normal to the MnO octahedral sheets, their structural similarity is revealed (Fig. 5). It is interesting to note that this migration of reduced Mn cations from the octahedral sheets to the interlayer parallels the similar behavior during the room-temperature transformation of triclinic birnessite to hexagonal birnessite at pH below  $\sim 5$ .

The mineral hetaerolite has the nominal formula ZnMn<sub>2</sub>O<sub>4</sub>, but as the spinel phase in our experiments was formed directly from anhydrous chalcophanite (and the diffraction patterns do not show other phases), the product of our heating experiment apparently retained the Zn/Mn ratio of the precursor phase, yielding the formula: (Zn<sub>0.75</sub>Mn<sub>0.25</sub><sup>2+</sup>)Mn<sub>2</sub><sup>3+</sup>O<sub>4</sub>. Thus, the dehydration of chalcophanite generated a compound whose chemistry lies one-quarter of the way along the compositional series between hetaerolite and hausmannite (Mn<sup>2+</sup>Mn<sub>3</sub><sup>3+</sup>O<sub>4</sub>). The refined

occupancy factor for the spinel Zn site was 0.94, as would be expected for a tetrahedral site with 75% Zn and 25% Mn. The refined Mn<sup>3+</sup>-O distances of 1.935 Å (×4) and 2.285 Å (×2) (Table 3) are the same as values reported for hausmannite (Baron et al. 1998) and reflect the Jahn-Teller distortion associated with Mn<sup>3+</sup>. The slightly larger tetrahedral (Zn,Mn)-O distance of 1.99 Å compared to the predicted value of 1.98 Å for Zn-O given above reflects the presence of the larger Mn<sup>2+</sup> cation (Mn<sup>2+</sup>-O = 2.03; Shannon 1976). The bond valence sum (Brown and Altermatt 1985) calculated for the octahedral Mn<sup>3+</sup>, using bond distances from Table 3, is 2.97, and for the tetrahedral Zn/Mn (weighting bond strengths proportional to Zn/Mn content) is 1.95.

### IMPLICATIONS

Time-resolved synchrotron powder diffraction studies of the dehydration of chalcophanite provides insights into the dehydration behavior of birnessite-like Mn oxide phases. The ability of Zn to accommodate tetrahedral and octahedral coordination is likely the key to the formation of a stable anhydrous chalcophanite phase. The transformation from the layer structure to a spinel phase appears to be triggered by loss of O atoms during heating, and consequent reduction of Mn. This work should guide selection of interlayer cations for designing anhydrous phyllo-manganate battery materials and provide a better understanding of the stabilities and compositions of natural phyllo-manganates.

### ACKNOWLEDGMENTS

Funding for this research was provided by NSF grants EAR07-45374 and EAR11-47728. Thanks go to Jonathan Hanson of the Brookhaven National Lab for his assistance with the diffraction experiments at beamline X7B at the NSLS. We are grateful for the very helpful comments from two anonymous reviewers and the assistance of associate editor Aaron Celestian. This research was carried out at the National Synchrotron Light Source, Brookhaven National Laboratory, which is supported by the U.S. Department of Energy, Division of Materials Sciences and Division of Chemical Sciences, under Contract No. DE-AC02-98CH10886.

### REFERENCES CITED

Bach, S., Pereira-Ramos, J.P., and Baffier, N. (1995) Synthesis and characterization of lamellar MnO<sub>2</sub> obtained from thermal decomposition of NaMnO<sub>4</sub> for rechargeable lithium cells. *Journal of Solid State Chemistry*, 120, 70–73.

Baron, V., Gutzmer, J., Rundlo, H., and Tellgren, R. (1998) The influence of iron substitution on the magnetic properties of hausmannite, Mn<sup>2+</sup>(Fe,Mn)<sup>3+</sup>O<sub>4</sub>. *American Mineralogist*, 83, 786–793.

Brown, I.D., and Altermatt, D. (1985) Bond-valence parameters obtained from a systematic analysis of the inorganic crystal structure database. *Acta Crystallographica*, B41, 244–247.

Brown, G.E., Sueno, S., and Prewitt, C.T. (1973) A new single-crystal heater for the precession camera and four-circle diffractometer. *American Mineralogist*, 58, 698–704.

Burns, R.G., and Burns, V.M. (1977) Mineralogy. In G.P. Glasby, Ed., *Marine Manganese Deposits*, p. 185–248. Elsevier, Amsterdam.

Cai, J., Liu, J., and Suib, S.L. (2002) Preparative parameters and framework dopant effects in the synthesis of layer-structure birnessite by air oxidation. *Chemistry of Materials*, 14, 2071–2077.

Dasgupta, D.R. (1974) Oriented transformation of chalcophanite during thermal treatment. *Zeitschrift für Kristallographie*, 139, 116–128.

Drits, V.A., Silvester, E., Gorskov, A.I., and Manceau, A. (1997) Structure of synthetic monoclinic Na-rich birnessite and hexagonal birnessite: I. Results from X-ray diffraction and selected-area electron diffraction. *American Mineralogist*, 82, 946–961.

Golden, D.C., Dixon, J.B., and Chen, C.C. (1986) Ion exchange, thermal transformations, and oxidizing properties of birnessite. *Clays and Clay Minerals*, 34, 511–520.

Grice, J.D., Gartrell, B., Gault, R.A., and Van Velthuisen, J. (1994) Ermenickelite,

NiMn<sub>2</sub>O<sub>7</sub>·3H<sub>2</sub>O, a new mineral species from the Siberia complex, Western Australia: comments on the crystallography of the chalcophanite group. *Canadian Mineralogist*, 32, 333–337.

Guiyin, Y., Shanghua, Z., Mingkai, Z., Jianping, D., and Deyu, L. (1992) Jianshuiite—A new magnesian mineral of chalcophanite group. *Acta Mineralogica Sinica* 12(1), 69–77 (in Chinese with English abstract).

Hammersley, A.P., Svensson, S.O., Hanfland, M., Fitch, A.N., and Hausermann, D. (1996) Two-dimensional detector software: From real detector to idealized image or two-theta scan. *High Pressure Research*, 14, 235–248.

Johnson, E.A., and Post, J.E. (2006) Water in the interlayer region of birnessite: importance in cation exchange and structural stability. *American Mineralogist*, 91, 609–619.

Jones, L.H.P., and Milne, A.A. (1956) Birnessite, a new manganese oxide mineral from Aberdeenshire, Scotland. *Mineralogical Magazine*, 31(235), 283–288.

Kwon, K.D., Refson, K., and Sposito, G. (2009) Zinc surface complexes on birnessite: A density functional theory study. *Geochimica et Cosmochimica Acta*, 73, 1273–1284.

Lanson, B., Drits, V.A., Feng, Q., and Manceau, A. (2002) Structure of synthetic Na-birnessite: Evidence for a triclinic one-layer cell. *American Mineralogist*, 87, 1662–1671.

Larson, A.C., and Von Dreele, R.B. (2006) GSAS-General Structure Analysis System. Los Alamos National Laboratory Report, LAUR 86-748.

Lopano, C.L., Heaney, P.J., Post, J.E., Hanson, J., and Komarneni, S. (2007) Time-resolved structural analysis of K- and Ba-exchanged reactions with synthetic Na-birnessite using synchrotron X-ray diffraction. *American Mineralogist*, 92, 380–387.

McKenzie, R.M. (1971) The synthesis of birnessite, cryptomelane, and some other oxides and hydroxides of manganese. *Mineralogical Magazine*, 38, 493–502.

——— (1976) The manganese oxides in soils. In I.M. Varentsov and G. Grassley, Eds., *Proceedings of the 2nd International Symposium on Geology and Geochemistry of Manganese*, 1, p. 259–269. Schweizerbart, Stuttgart.

——— (1977) Manganese oxides and hydroxides. In J.B. Dixon and S.B. Weed, Eds., *Minerals in Soil Environments*, p. 181–193. Soil Science Society of America, Madison, Wisconsin.

Post, J.E. (1999) Manganese oxide minerals: Crystal structures and economic and environmental significance. *Proceedings of the National Academy of Sciences*, 96, 3447–3454.

Post, J.E., and Appleman, D.E. (1988) Chalcophanite, ZnMn<sub>2</sub>O<sub>7</sub>·3H<sub>2</sub>O: New crystal-structure determinations. *American Mineralogist*, 73, 1401–1404.

Post, J.E., and Bish, D.L. (1989) Rietveld refinement of crystal structures using powder X-ray diffraction data. In D.L. Bish and J.E. Post, Eds., *Modern Powder Diffraction*, vol. 20, p. 277–308. Reviews in Mineralogy, Mineralogical Society of America, Chantilly, Virginia.

Post, J.E., Heaney, P.J., and Hanson, J. (2002) Rietveld refinement of a triclinic structure for synthetic Na-birnessite using synchrotron powder diffraction data. *Powder Diffraction*, 17, 218–221.

Post, J.E., Heaney, P.J., and Ertl, A. (2008) Rietveld refinement of the ranciéite structure using synchrotron powder diffraction data. *Powder Diffraction*, 23, 10–14.

Potter, R.M., and Rossman, G.R. (1979) Mineralogy of manganese dendrites and coatings. *American Mineralogist*, 64, 1219–1226.

Shannon, R.D. (1976) Revised effective ionic radii and systematic studies of interatomic distances in halides and chalcogenides. *Acta Crystallographica* A32, 751–767.

Stephens, P.W. (1999) Phenomenological model of anisotropic peak broadening in powder diffraction. *Journal of Applied Crystallography*, 32, 281–289.

Taylor, R.M., McKenzie, R.M., and Norrish, K. (1964) The mineralogy and chemistry of manganese in some Australian soils. *Australian Journal of Soil Research*, 2, 235–248.

Thompson, P., Cox, D.E., and Hastings, J.B. (1987) Rietveld refinement of Debye-Scherrer synchrotron X-ray data from Al<sub>2</sub>O<sub>3</sub>. *Journal of Applied Crystallography*, 20, 79–83.

Toby, B.H. (2001) EXPGUI, a graphical user interface for GSAS. *Journal of Applied Crystallography*, 34, 210–213.

Toner, B., Manceau, A., Webb, S.M., and Sposito, G. (2006) Zinc sorption to biogenic hexagonal-birnessite particles within a hydrated bacterial biofilm. *Geochimica et Cosmochimica Acta*, 70, 27–43.

Wadsley, A.D. (1955) The crystal structure of chalcophanite, ZnMn<sub>2</sub>O<sub>7</sub>·3H<sub>2</sub>O. *Acta Crystallographica*, 8, 165–172.

MANUSCRIPT RECEIVED SEPTEMBER 30, 2013

MANUSCRIPT ACCEPTED APRIL 21, 2014

MANUSCRIPT HANDLED BY AARON CELESTIAN